

PACS numbers: 78.47.J–; 63.20.kd; 63.20.dd; 42.25.Kb
DOI: 10.1070/QE2013v043n04ABEH015108

Ultrafast broadband spectroscopy of crystalline bismuth

A.A. Melnikov, O.V. Misochko, S.V. Chekalin

Abstract. **Femtosecond spectroscopy in the wavelength range 0.4–2.3 μm has been used to probe ultrafast electronic and lattice processes in bismuth. The photoresponse of a bismuth crystal is shown to comprise components with relaxation times of 1 ps, 7 ps, and ~1 ns. The electron–hole and electron–phonon interaction strengths in bismuth are found to depend significantly on the wave vector in the Γ–T direction of the Brillouin zone. Comparison of the spectral dependences of the amplitudes of coherent E_g and A_{1g} phonons and the corresponding dependences of the Raman scattering cross sections indicates that these phonon modes differ in generation mechanism. The generation of coherent A_{1g} phonons is mainly due to displacement of the equilibrium position of atoms in the crystal lattice in a nonequilibrium state. This process differs fundamentally from resonance Raman scattering responsible for the coherent excitation of low-symmetry phonon modes.**

Keywords: *femtosecond spectroscopy, electron–phonon coupling, bismuth, coherent phonons.*

1. Introduction

In the past two decades, both theorists and experimentalists have paid a great deal of attention to the interaction of ultrashort laser pulses with solids. Constant interest in this issue is generated primarily by the fact that the range from femto- to nanoseconds, investigated by standard ultrafast optical techniques, includes characteristic times of fundamental processes, such as electron thermalisation, electron–phonon relaxation, formation and decay of collective excitations (excitons, polarons, magnons and others), phase transitions and many others.

A special place is held by the use of ultrashort laser pulses for probing opaque crystals. The laser energy is then absorbed by electrons within ~10 fs, a time short compared to the characteristic period of atomic motion (~100 fs at room temperature). As a result, the interatomic potential of the solid changes significantly, especially under the action of high-power femtosecond pulses. The relaxation of highly nonequilibrium states of this kind may be accompanied by unusual effects, including ultrafast atomic disordering (or nonthermal melting), ultrafast structural transitions of solids and 'coherent' phonon (CP) generation.

The ability to determine the modified interatomic potential and predict further evolution of the electron and lattice subsystems of the crystal is a challenging problem in the theory of solids. As a result, simplified or even phenomenological approaches are often used in interpreting experimental data.

One example is the so-called two-temperature model [1], which is widely used to interpret the kinetics of photoexcited electrons in semiconductors and metals. According to this model, femtosecond laser radiation is absorbed by some of the valence electrons, producing a nonequilibrium electron distribution. Electron–electron interaction leads to energy redistribution between all charge carriers, following which a particular electron temperature T_e sets in. This process, commonly referred to as thermalisation, lasts from a few to tens of femtoseconds. Therefore, at the end of a pump pulse, the crystal lattice is at room temperature, T_0, whereas the electron subsystem has a temperature $T_e \gg T_0$. The subsequent process is energy transfer from the 'hot' electron ensemble to the 'cold' lattice through electron–phonon coupling over a period considerably longer than the thermalisation time. Thus, an excited state of a crystal can be characterised by the total number of photoexcited electrons or their temperature.

One prominent example that casts doubt on the applicability of this approach is crystalline bismuth. The relaxation of the nonequilibrium electron distribution in this material is accompanied not only by heating of its crystal lattice but also by intense correlated atomic vibrations of certain spatial symmetry. The frequency of such vibrations is as a rule close to the frequency of the A_{1g} phonon mode of bismuth, so the process in question is referred to as CP generation in the crystal [2, 3].

Currently, CPs in bismuth are being actively studied in the context of possible structural quantum effects. The ability to detect correlated vibrations allows one to gain insight into electron–phonon coupling, phonon anharmonicity [4] and laser field coherence transfer to the crystal lattice. Intriguing assumptions have been made that one can create squeezed and entangled phonon states [5] and a transient Bose–Einstein condensate of phonons [6]. Note that not only essentially quantum-mechanical phenomena but even the observation of coherent atomic vibrations cast doubt on whether thermodynamic models of relaxation similar to the two-temperature model are applicable to bismuth [2, 7, 8].

Another distinctive feature of bismuth is that it has unusual electronic properties. Bismuth is a semimetal and has an indirect overlap of its valence and conduction bands [9]. Because of this, depending on photon energy a laser pulse

A.A. Melnikov, S.V. Chekalin Institute of Spectroscopy, Russian Academy of Sciences, Fizicheskaya ul. 5, 142190 Troitsk, Moscow, Russia; e-mail: melnikov@isan.troitsk.ru;
O.V. Misochko Institute of Solid State Physics, Russian Academy of Sciences, ul. Akad. Osip'yana 2, 142432 Chernogolovka, Moscow region, Russia

Received 24 December 2012; revision received 10 February 2013
Kvantovaya Elektronika **43** (4) 313–319 (2013)
Translated by O.M. Tsarev

may cause 'interband' and 'intraband' electronic transitions, similar to those in semiconductors and metals, respectively. Since different energy levels become filled in these transitions, the relaxation of nonequilibrium states in bismuth is a relatively complex process [10].

The use of simplified models for interpreting ultrafast processes in bismuth is in many respects caused by the character of available data. In almost all studies, so-called degenerate pump–probe measurements were used to gain insight into ultrafast phenomena in bismuth. The processes of interest are initiated by a pump pulse and are detected using a time-delayed probe pulse to measure the transmission or reflectivity of the sample. Both laser pulses reproduce the input pulse and, hence, their relatively narrow spectrum is centred at the same wavelength. As a result, there is a photoresponse at only one wavelength and the evolution of the nonequilibrium state is difficult to interpret unambiguously. In a number of studies, bismuth was probed by X-ray [11, 12] or electron diffraction [13, 14] and angle-resolved electron spectroscopy [15]. In the former case, however, essentially no information about the dynamics of outer electrons is provided and, in the latter, surface states are primarily probed.

In this study, the photoresponse of bismuth is examined for the first time in the visible and near-IR spectral regions. Near-IR excitation is shown to slow down the electron dynamics in bismuth and initiate the generation of CPs of the E_{1g} (doubly degenerate) mode, along with A_{1g} (totally symmetric) vibrations [16]. Our data on the decay of nonequilibrium excited states demonstrate that there are several groups of charge carriers that differ markedly in relaxation time, which invalidates the concept of a fully thermalised ensemble of electrons that determines the photoresponse of bismuth. Various groups of charge carriers are assigned to particular regions in the Brillouin zone, electron–phonon coupling strength is evaluated for electronic states with the corresponding wave vectors, and the generation mechanisms are identified for CPs of various spatial symmetries.

2. Experimental details

In our experiments, we employed a standard pump–probe technique, with femtosecond pulses generated by a Ti:sapphire laser at wavelengths λ = 800 and 400 nm (after frequency doubling in a BBO crystal) or λ = 600–2300 nm (after parametric amplification). The pump pulse duration was ~70 fs. In addition, supercontinuum pulses (λ = 450–780 nm) were used as probes. The pump and probe pulses were focused onto the surface of a bismuth single crystal cleaved along the (111) plane. The spot diameter of the pump laser beam on the crystal surface exceeded that of the probe beam. We measured the relative reflectivity change $\Delta R(t)/R$ as a function of pump–probe delay time t. Two measurement systems were used: multichannel (resolution, 250 fs; sensitivity, $\sim 10^{-4}\Delta R/R$), with broadband supercontinuum detection by linear photodiode arrays, and single-channel (resolution, 100 fs; sensitivity, $\sim 10^{-5}\Delta R/R$), with narrow-band detection by individual photodiodes. All the measurements were made at room temperature and atmospheric pressure.

3. Results and discussion

The photoresponse of bismuth (Fig. 1) comprises a monotonic signal and damped oscillations. These latter are caused by CPs of A_{1g} symmetry, whereas the monotonic component represents the relaxation of photoexcited carriers and incoherent (thermal) processes in the crystal lattice. In experiments, such CPs can be detected only indirectly, but comparison with X-ray measurement results in a previous study [17] indicates that the optical pump–probe technique gives adequate CP parameters: the frequency, phase and decay time.

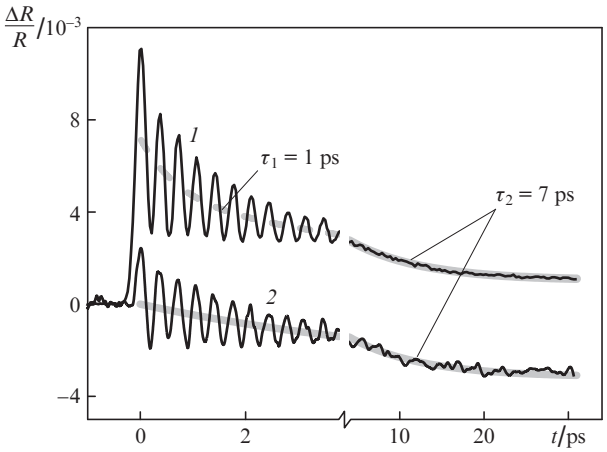

Figure 1. Photoresponse $\Delta R/R$ of bismuth measured at wavelengths of (*1*) 780 and (*2*) 600 nm with the single-channel system using 400-nm pump pulses with a fluence of 1.3 mJ cm^{-2}. The solid lines represent the slow component of the electronic response and the dashed line represents the fast component.

The total photoresponse of bismuth, shown in Fig. 1 for two probe wavelengths, can be represented as

$$\Delta R/R = A\exp(-\gamma t)\cos[\nu_A(t)t] + (\Delta R/R)_{mon}, \quad (1)$$

where A is the amplitude and $\gamma \approx 0.5$ ps^{-1} is the decay rate of the A_{1g} oscillations. The monotonic component of the signal, $(\Delta R/R)_{mon}$, can be represented in the form

$$(\Delta R/R)_{mon} = \sigma_1\exp(-t/\tau_1) + \sigma_2\exp(-t/\tau_2) + \sigma_3, \quad (2)$$

where σ_1, σ_2 and σ_3 are the contributions of components at a given probe wavelength (the time delay t is in picoseconds). Strictly speaking, σ_3 should also be multiplied by an exponential, but its decay time is so long (~1 ns according to our measurements) that the approximation we use is accurate enough for a period of 30 ps. The above components correspond to several groups of electrons with different relaxation rates, which are determined primarily by electron–phonon coupling efficiency.

The oscillation amplitude and the contributions of the fastest and quasi-constant components are wavelength-dependent. At the same time, the instantaneous frequency and lifetime of the vibrations are independent of the probe wavelength at a given excitation intensity and wavelength. Representing the monotonic photoresponse of bismuth at two wavelengths by (2), we obtained $\tau_1 = 1.0 \pm 0.5$ ps, $\tau_2 = 7.0 \pm 0.5$ ps and $\sigma_2 \approx 0.007$ over the entire range of probe wavelengths studied. Figure 2 shows σ_1, σ_3 and A as functions of probe wavelength.

One incoherent process that can underlie the above data is energy transfer from excited electrons to the crystal lattice,

similar to what occurs in metals. This process shows up as a reduction in reflectivity, uniform throughout the visible range (σ_2 is wavelength-independent), with a relaxation time of 7 ps. The reflectivity of bismuth is known to decrease with increasing temperature [18], and the decrease is uniform over the spectrum. It is therefore reasonable to assign the σ_2 component to the heating of the crystal due to the interaction of its lattice with some of the excited electrons. Using earlier data [19], we can estimate the increase in temperature in our case. Wu and Xu [19] obtained $d(\Delta R/R)/dT = 8.5\times10^{-5}$ K^{-1}. Dividing $\sigma_2 = 0.007$ by this value, we find that, ~20 ps after heating is ceased, the temperature of the crystal is 383 K. It is worth noting that this temperature is substantially lower than the melting point of bismuth (490 K). The above estimate indicates that, at the excitation fluence used in our experiments (~1–2 mJ cm^{-2}), bismuth is crystalline throughout the relaxation process.

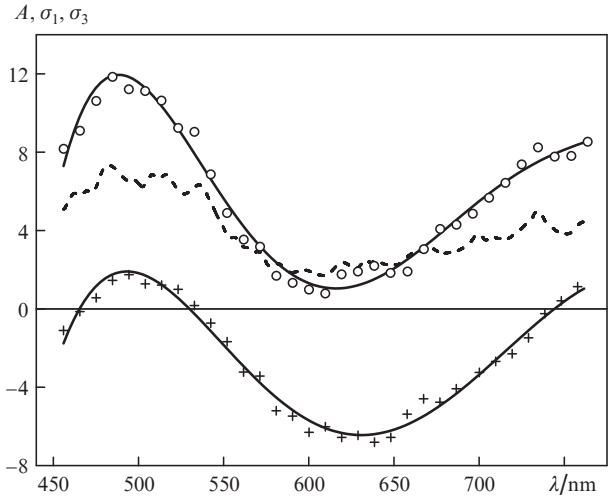

Figure 2. Spectra of the amplitude A of coherent oscillations (dashed line) and the fast (σ_1, o) and quasi-constant (σ_3, +) components of the monotonic photoresponse (data extracted from multichannel measurement results).

Since $\Delta R/R \neq 0$ at long delay times, the relaxation process in crystalline bismuth does not cease after heating. The residual signal is determined by the slow component $\sigma_3(\lambda)$, whose nanosecond dynamics are characteristic of semiconductors. In semiconductors, electrons excited by ultrashort laser pulses to the conduction band rapidly occupy states near its bottom, and the characteristic time of subsequent electron–hole recombination typically lies in the nanosecond range. Even though bismuth is not a semiconductor but a semimetal, with its valence and conduction bands overlapping each other, the overlap is indirect and the electron–hole recombination near the Fermi level is a rather slow process [20]. Thus, the $\sigma_3(\lambda)$ component is attributable to nonequilibrium electrons that occupy states in the conduction band near the Fermi level. Note that the recombination of these charge carriers makes no significant contribution to the heating of the sample because it occurs simultaneously with the heat diffusion to the interior of the crystal, whose characteristic time also lies in the nanosecond range.

An important point is that the $\sigma_3(\lambda)$ spectrum is similar in shape to the spectral dependence of the coherent amplitude. Indeed, it is seen in Fig. 2 that both spectra have a minimum near $\lambda = 620$ nm. The coincidence is rather interesting and can be interpreted as follows.

A_{1g} vibrations are known to be antiphase vibrations of two atoms that constitute a unit cell of bismuth along its trigonal axis [21, 22]. The equilibrium distance between these atoms is often referred to as an internal displacement, δ. The δ value determines the distinction of the rhombohedral structure of bismuth from a cubic structure and the indirect overlap of its valence and conduction bands. Because of this, the free carrier concentration depends on δ. Since the number of free carriers influences the intensity of the light reflected from the crystal, a change in internal displacement, $\Delta\delta$, leads to an increase or decrease in reflectivity, ΔR. CPs of A_{1g} symmetry correspond to a periodic modulation of δ and, accordingly, show up as reflectivity oscillations with a wavelength-dependent amplitude $A(\lambda)$. Another way to change the number of free carriers, in addition to changes in δ, is to fill states near the Fermi level using photons. It is possible with femtosecond excitation because the excited electrons lose their energy and some of them accumulate near the Fermi level. Their contribution to the photoresponse is represented by the nanosecond component σ_3, whose spectrum in the case under consideration should have common features with the spectrum of the A_{1g} oscillation amplitude. This is what is observed: the $\sigma_3(\lambda)$ and $A(\lambda)$ spectra are similar in shape. The minimum in both spectra at $\lambda = 620$ nm (2 eV) may be due to the influence of the $L_a(2)$–$L_s(3)$ interband transition (in the notation proposed by Wang and Jain [23]), with an energy of 1.92 eV.

Consider another important correlation found in our experiments. The instantaneous frequency of coherent A_{1g} phonons, ν_A, varies with time, which is due to the effect of excited electrons on the interatomic potential of the bismuth crystal. At a near-zero delay time, ν_A is lower than the steady-state frequency ν_0 obtained in Raman measurements (so-called frequency softening, or bond softening). As shown previously [17],

$$\nu_A(t) \approx \nu_0 + \Delta\nu\exp(-t/\tau), \qquad (3)$$

where $\nu_0 = 2.93$ THz; $\tau = 1\pm0.3$ ps; and $\Delta\nu$ is the excitation-intensity-dependent frequency change due to the softening effect. Thus, the characteristic relaxation time of the instantaneous frequency of A_{1g} vibrations coincides with that of the fast component σ_1 of the monotonic response to within the present measurement accuracy. This suggests that there is strong coupling between the A_{1g} phonon mode and the group of electrons with picosecond dynamics. To find out where in the Brillouin zone these nonequilibrium charge carriers are located, we used near-IR femtosecond pump pulses. The pump wavelength was varied in the range 400 to 2300 nm. In each case, we took into account the pump beam spot diameter on the sample surface and the reflectivity of bismuth at a particular wavelength in order to ensure a constant excitation intensity (optical field intensity in the surface layer of the sample) throughout the spectral range studied. When this condition was satisfied, the amplitudes of the picosecond ($\tau_2 = 7$ ps) and nanosecond components were essentially independent of the pump wavelength. This is well seen in Fig. 3, which compares the photoresponses measured using femtosecond pulses at $\lambda = 400$ and 2300 nm. After ~4 ps, the curves almost coincide, whereas at shorter delay times they differ markedly, which is primarily due to the smaller amplitude of

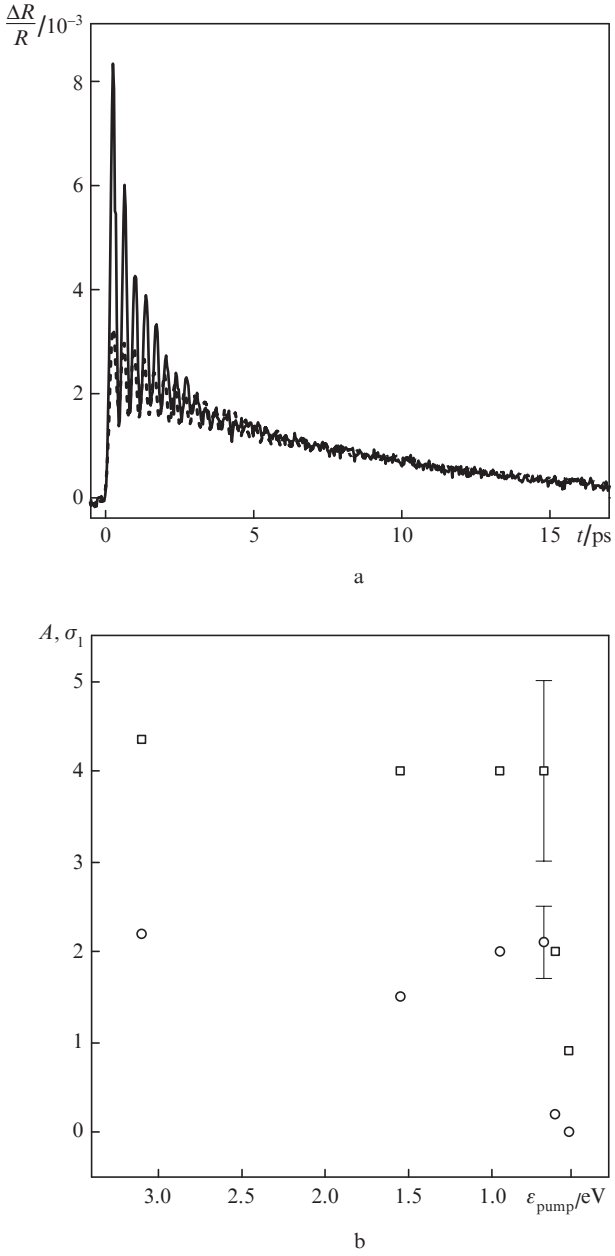

Figure 3. (a) Photoresponse of bismuth at a probe wavelength of 800 nm under pulsed excitation at $\lambda = 400$ (solid line) and 2300 nm (dashed line). (b) Initial oscillation amplitude A (□) and amplitude of the σ_1 component with $\tau_1 = 1$ ps (○) as functions of pump photon energy.

coherent oscillations and smaller contribution of the component with $\tau_1 = 1$ ps under IR excitation. Moreover, a detailed analysis indicates that the longer wavelength excitation leads to a smaller phonon frequency shift.

The oscillation amplitude and the contribution of the component with $\tau_1 = 1$ ps were measured as functions of pump photon energy in the range 0.5–3 eV. To reach the best sensitivity, the measurements were made with the single-channel system at a probe wavelength of 800 nm. The results (Fig. 3b) demonstrate that the amplitude of CPs and that of the σ_1 component are similar in behaviour: both decrease considerably at pump photon energies below ~0.7 eV.

To relate this energy to the electronic properties of bismuth, we used the band structure parameters of bismuth calculated by Golin [24]. The energy of 0.7 eV approaches the energies of the $\Gamma_6^+(5)-\Gamma_6^-(6)$ and $\Gamma_{45}^+(4)-\Gamma_6^-(6)$ optical transitions: 0.821 and 0.825 eV [24]. In piezoreflectance experiments [23], the respective values were 0.69 and 0.81 eV, so it is reasonable to assign the σ_1 component to excited electrons that occupy states in the band containing point Γ_6^- (Fig. 4). Thus, when the pump photon energy exceeds 0.7 eV, electrons can occupy these states either directly or through relaxation from higher energy levels due to electron–electron interaction. The relaxation time is substantially shorter than the time resolution in our experiments, as evidenced by the similarity of the photoresponses under excitation in the visible spectral regions.

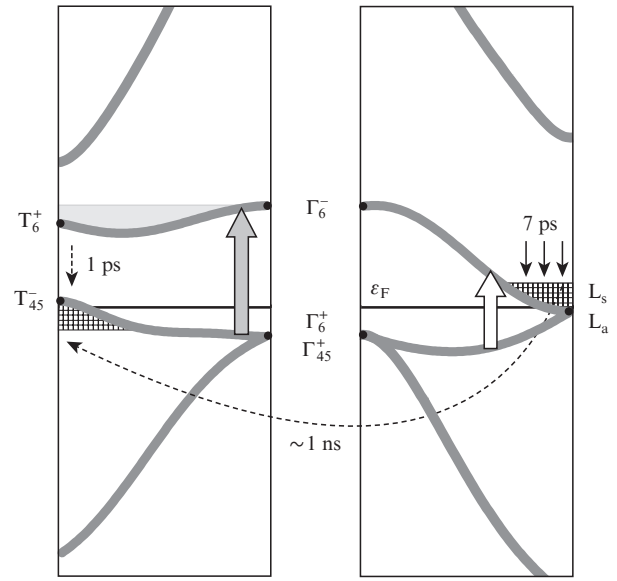

Figure 4. Portion of the band structure of bismuth from Ref. [23]. The grey arrow represents resonance electron excitation resulting in the component with $\tau_1 = 1$ ps and A_{1g} phonon generation. The open arrow represents intraband transitions which cause only charge accumulation near the Fermi level. The cross-hatched areas represent excited electrons and holes with nanosecond lifetimes at points L and T.

It is important here to take into account as well the decrease in phonon frequency shift with increasing pump wavelength. This result indicates that excited electrons in the band containing point Γ_6^- cause significant A_{1g} mode softening. Since A_{1g} in bismuth is a Peierls distortion mode, it is reasonable to draw an analogy with quasi-one-dimensional materials. Indeed, in materials characterised by a Peierls distortion of the crystal lattice, strong coupling would be expected between longitudinal optical phonons in the centre of the Brillouin zone and electronic states at its periphery. In bismuth, the internal displacement δ, which is an order parameter of the Peierls phase, is parallel to the trigonal axis, which corresponds to the $\Gamma-\Lambda-T$ direction in reciprocal space. In this case, the longitudinal optical phonons that modulate δ are A_{1g} phonons in the form of a coherent wave packet composed of states near the centre of the Brillouin zone. Thus, it follows from the above analogy that excited electrons responsible for the σ_1 component occupy states near point T_6^+ in the Brillouin zone of bismuth.

The electronic states that are excited at photon energies below 0.7 eV are characterised by picosecond (~7 ps) 'cooling' (by analogy with metals) and nanosecond relaxation (see Fig. 4).

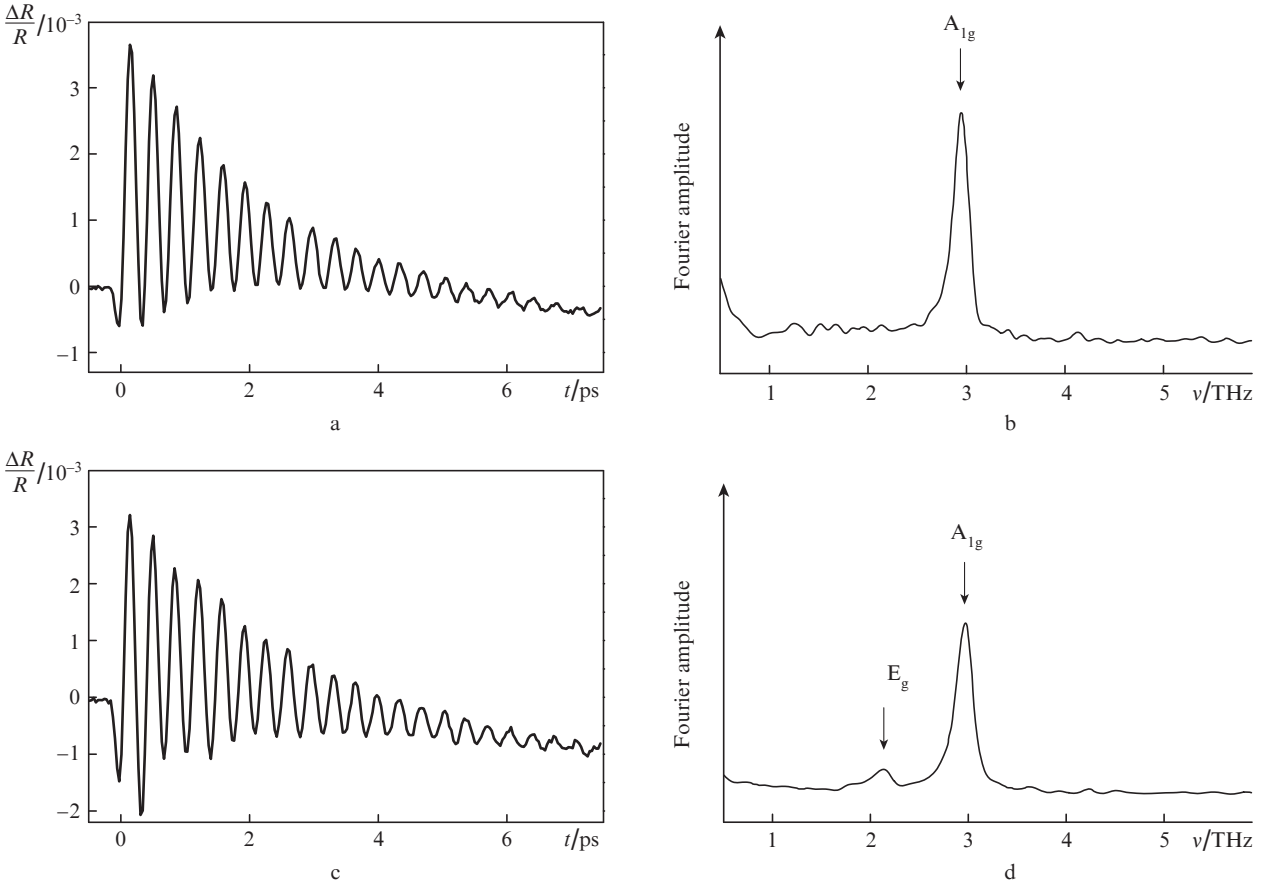

Figure 5. Relative reflectivity change as a function of time delay for bismuth under excitation with (a) 400- and (c) 1300-nm pulses. (b, d) Normalised Fourier spectra of the oscillating component of the signal for panels (a) and (c), respectively.

It is reasonable to identify these charge carriers as nonequilibrium electrons and holes at points L and T, respectively, near the Fermi level. The relaxation with a characteristic time of ~1 ns is then their indirect recombination.

Varying the pump pulse wavelength leads not only to a reduction in the oscillation amplitude of coherent A_{1g} phonons and in electron relaxation rate but also to another interesting effect. It can be observed at lower excitation fluences (~0.1 mJ cm^{-2}).

Figure 5 shows the relative reflectivity change as a function of time delay for bismuth under excitation with 400- and 1300-nm pulses (excitation fluence, ~0.3 mJ cm^{-2}). The Fourier spectra presented in Figs 5b and d demonstrate that the principal distinction between the curves in Fig. 5 is the presence of strongly damped 2.1-THz oscillations, which are attributable to coherent phonons of E_g symmetry [4, 25]. With E_g vibrations included in analysis, a good fit to these curves can be obtained.

Figure 6 shows the spectral dependences of the amplitude for the totally symmetric and doubly degenerate phonon modes. The amplitude of the E_g oscillations is seen to be almost zero in the visible range (at pump wavelengths λ = 400, 600 and 700 nm). At the same time, at $\lambda \sim 800$ nm the E_g mode amplitude begins to rise, reaching a maximum near λ = 1300 nm (~1 eV). In contrast, the A_{1g} phonon amplitude is roughly constant in the visible and near-IR spectral regions, up to λ = 1300 nm. At pump wavelengths above λ = 1800 nm (~0.7 eV), the generation efficiency of the two phonon modes drops significantly.

The result obtained is remarkable in that it demonstrates the feasibility of observing relatively strong coherent E_g phonons (the E_g amplitude is one-quarter of the A_{1g} amplitude) even in standard pump–probe experiments at room temperature by using an appropriate pump wavelength. In previous studies, the photoresponse was dominated by totally symmetric CPs, and doubly degenerate CPs were only detected at low temperatures [25] or high excitation fluences [4], or when anisotropic detection was used [26]. The efficient E_g phonon generation is obviously the consequence of the resonance character of the process, as supported by the shape of the spectral dependence of the E_g amplitude (Fig. 6).

It is now worth turning to existing models for the band structure of bismuth in order to attempt to identify which electronic transitions are responsible for the observed resonance near ε_{pump} = 1 eV. As above, theoretical results [24] and experimental piezoreflectance data [23] can be used for this purpose. It is worth noting that the femtosecond pulses employed in our measurements had a rather broad spectrum. The same refers to the width of the electronic bands involved in optical transitions in bismuth. Because of this, the A_{1g} and E_g resonances can be interpreted in several ways. According to Golin [24], these are the $L_a(5)-L_s(7)$, $\Gamma^+_{45}(4)-\Gamma^-_6(6)$ and $\Gamma^+_6(5)-\Gamma^-_6(6)$ transitions, with energies of 1.15, 0.825 and 0.821 eV, respectively. Slightly lower values were extracted from piezoreflectance data: 1.13, 0.81 and 0.69 eV [23]. In this case, the maximum in the E_g amplitude corresponds to one of the above transitions. When the carrier frequency of a femtosecond pump pulse approaches the frequency of a tran-

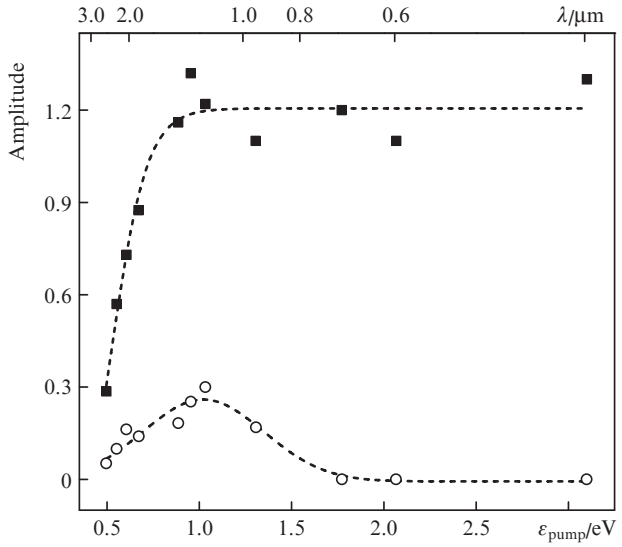

Figure 6. Amplitudes of A_{1g} (■) and E_g (○) coherent oscillations as functions of pump photon energy.

sition, the CP generation efficiency rises steeply. If the frequency is detuned from resonance, the efficiency drops and the E_g mode is essentially impossible to detect by a standard pump–probe technique.

The description of CP generation in terms of a generalised Raman scattering model [27, 28] suggests that the coherent oscillation phase in the case of resonance should be $\pi/2$, which corresponds to a cosinusoidal time dependence. In bismuth, resonance conditions are realised for both the A_{1g} and E_g modes, so the initial phase shift of the two modes in this model should be taken to be zero. However, analysis of our experimental data indicates a 90° phase difference at λ = 1300 nm and at any pump wavelength at which we were able to measure the E_g oscillation amplitude [16].

Clearly, this result is at variance with the simplest version of the generalised Raman scattering model, but the contradiction can be eliminated by taking into account the finite carrier lifetime, as was done by Riffe and Sabbah [29]. To this end, the lifetime of charge carriers associated with E_g phonons should be assumed to be much shorter than the pump pulse duration. In addition, the carrier concentration should be anisotropic to satisfy symmetry constraints.

There is, however, a serious argument against applying any version of the generalised Raman scattering model to totally symmetric vibrations. In a previous study [16], we compared the amplitudes of the A_{1g} and E_g modes obtained in our time-resolved experiments to the corresponding Raman scattering cross sections measured in the range ε_{pump} = 1.55–2.7 eV [30]. The results demonstrate that only for the E_g mode do the Raman scattering cross section and CP amplitude vary similarly with pump wavelength. The spectral range used by Renucci et al. [30] was too narrow to find the exact resonance position of the E_g mode. Nevertheless, they assumed that Raman scattering would be most efficient at photon energies near the energy at the critical point E_1 of bismuth (1.2 eV) [30]. This point corresponds to the above-mentioned transition $L_a(5)-L_s(7)$.

In contrast to the E_g oscillations, coherent A_{1g} phonons are effectively generated only when the pump photon energy exceeds a critical value, which was determined to be ~0.7 eV. When this condition is met, the amplitude and even the entire photoresponse are essentially independent of pump wavelength. The observed distinction between the Raman A_{1g} resonance profile and the pump wavelength dependence of the amplitude of coherent A_{1g} phonons leads us to conclude that phonon generation through Raman scattering is inefficient in the case of totally symmetric phonons in bismuth.

The key role of absorbed energy and the unusually high efficiency of totally symmetric CP generation lead us to conclude that, in this case, the generation mechanism is displacement of the equilibrium position of atoms in the crystal lattice (displacive excitation of coherent phonons (DECP)). This process involves the modification of the interatomic potential due to energy redistribution between highly nonequilibrium charge carriers and carrier accumulation near point T_6^+ in the Brillouin zone. Since the characteristic time of electron–electron interaction is shorter than the A_{1g} vibration period, coherent atomic vibrations can be generated.

4. Conclusions

An ultrafast response of a bismuth single crystal to a femtosecond laser pulse has been measured in a broad spectral range. In contrast to simple models that describe a nonequilibrium state of bismuth by the total number of excited electrons, multicomponent electron dynamics were observed, with characteristic times from pico- to nanoseconds. Several groups of photoexcited charge carriers were identified, with different strengths of coupling to the crystal lattice. The most efficient coupling is that of electronic states near point T in the Brillouin zone to optical A_{1g} phonons at its centre. Incoherent dynamics are shown to involve heating of the crystal lattice in ~7 ps and nanosecond indirect electron–hole recombination near the Fermi level. Resonance amplification of the amplitude of the E_g mode has been demonstrated at a pump photon energy of ~1 eV. The spectral dependences of the amplitudes of the A_{1g} and E_g modes have been compared to experimental Raman scattering data. The results lead us to conclude that the generation of A_{1g} phonons is caused by displacement of the equilibrium position of atoms in the crystal lattice. The generation of E_g phonons is due to resonance Raman scattering.

Acknowledgements. This work was supported by the Presidium of the Russian Academy of Sciences (Extreme Light Fields and Their Applications Programme) and the Russian Foundation for Basic Research (Grant No. 12-02-00898a).

References

1. Allen P.B. *Phys. Rev. Lett.*, **59**, 1460 (1987).
2. Zeiger H., Vidal J., Cheng T., Ippen E., Dresselhaus G., Dresselhaus M. *Phys. Rev. B*, **45**, 768 (1992).
3. Hase M., Mizoguchi K., Harima H., Nakashima S., Sakai K. *Phys. Rev. B*, **58**, 5448 (1998).
4. Hase M., Kitajima M., Nakashima S., Mizoguchi K. *Phys. Rev. Lett.*, **88**, 067401 (2002).
5. Johnson S., Beaud P., Vorobeva E., Milne C., Murray É., Fahy S., Ingold G. *Phys. Rev. Lett.*, **102**, 175503 (2009).
6. Misochko O.V., Hase M., Ishioka K., Kitajima M. *Phys. Lett. A*, **321**, 381 (2004).
7. Boschetto D. et al. *Phys. Rev. Lett.*, **100**, 027404 (2008).
8. Giret Y., Gelle A., Arnaud B. *Phys. Rev. Lett.*, **106**, 155503 (2011).
9. Shick A., Ketterson J., Novikov D., Freeman A. *Phys. Rev. B*, **60**, 15484 (1999).
10. Melnikov A.A., Misochko O.V., Kompanets V.O., Dobryakov A.L., Chekalin S.V. *Zh. Eksp. Teor. Fiz.*, **138** (3), 486 (2010).
11. Fritz D.M. et al. *Science*, **315**, 633 (2007).

12. Johnson S. et al. *Phys. Rev. Lett*., **100**, 155501 (2008).
13. Sciaini G. et al. *Nature*, **458**, 56 (2009).
14. Esmail A.R., Elsayed-ali H.E. *Appl. Phys. Lett*., **99**, 161905 (2011).
15. Papalazarou E. et al. *Phys. Rev. Lett.*, **108**, 256808 (2012).
16. Melnikov A.A., Misochko O.V., Chekalin S.V. *Phys. Lett. A*, **375**, 2017 (2011).
17. Mel'nikov A.A., Misochko O.V., Chekalin S.V. *Pis'ma Zh. Eksp. Teor. Fiz.*, **89** (3), 148 (2009).
18. Cardona M., Greenaway D. *Phys. Rev*., **133**, A1685 (1964).
19. Wu A.Q., Xu X. *Appl. Phys. Lett*., **90**, 251111 (2007).
20. Lopez A. *Phys. Rev.*, **175**, 823 (1968).
21. Edel'man V.S. *Usp. Fiz. Nauk*, **123**, 257 (1977).
22. Fal'kovskii L.A. *Usp. Fiz. Nauk*, **99**, 3 (1968).
23. Wang P., Jain A. *Phys. Rev. B*, **2**, 2978 (1970).
24. Golin S. *Phys. Rev*., **166**, 643 (1968).
25. Ishioka K., Kitajima M., Misochko O.V. *J. Appl. Phys.*, **100**, 093501 (2006).
26. Hase M., Mizoguchi K., Harima H., Nakashima S. *Appl. Phys. Lett*., **69**, 2474 (1996).
27. Garrett G., Albrecht T., Whitaker J., Merlin R. *Phys. Rev. Lett*., **77**, 3661 (1996).
28. Stevens T., Kuhl J., Merlin R. *Phys. Rev. B*, **65**, 144304 (2002).
29. Riffe D., Sabbah A. *Phys. Rev. B*, **76**, 085207 (2007).
30. Renucci J.B., Richter W., Cardona M., Schöstherr E. *Phys. Status Solidi B*, **60**, 299 (1973).